Journal of Orthopaedic Translation 20 (2020) 25–30

Contents lists available at ScienceDirect

Journal of Orthopaedic Translation

journal homepage: www.journals.elsevier.com/journal-of-orthopaedic-translation

Original Article

Design of a new magnesium-based anterior cruciate ligament interference screw using finite element analysis

Jonquil R. Mau [a,b], Kevin M. Hawkins [a], Savio L.-Y. Woo [b], Kwang E. Kim [b], Matthew B.A. McCullough [a,*]

[a] Department of Chemical, Biological, and Bioengineering, North Carolina A&T State University, Greensboro, NC, USA
[b] Musculoskeletal Research Center, Department of Bioengineering, Swanson School of Engineering, University of Pittsburgh, Pittsburgh, PA, USA

ARTICLE INFO

Keywords:
Finite element analysis
Interference screw
Screw design
Screw insertion

ABSTRACT

Background/objective: In anterior cruciate ligament reconstruction, a tendon graft, anchored by interference screws (IFSs), is frequently used as a replacement for the damaged ligament. Generally, IFSs are classified as being either metallic or polymeric. Metallic screws have sharp threads that lacerate the graft, preventing solid fixation. These constructs are difficult to image and can limit bone–screw integration because of the higher stiffness of the screw. Polymeric materials are often a better match to bone's material properties, but lack the strength needed to hold grafts in place. Magnesium (Mg) is a material of great promise for orthopaedic applications. Mg has mechanical properties similar to bone, ability to be seen on magnetic resonance imagings, and promotes bone healing. However, questions still remain regarding the strength of Mg-based screws. Previous *ex vivo* animal experiments found stripping of the screw drive when the full torque was applied to Mg screws during surgery, preventing full insertion and poor graft fixation. The similar design of the Mg screw led to questions regarding the relationship between material properties and design, and the ultimate impact on mechanical behaviour. Thus, the objective of this study was to analyze the stresses in the screw head, a key factor in the stripping mechanism of IFS, then use that information to improve screw design, for this material.

Methods: Using finite element analysis, a comparison study of six drive designs (hexagonal, quadrangle, torx, trigonal, trilobe, and turbine) was performed. This was followed by a parametric analysis to determine appropriate drive depth and drive width.

Results: It was observed that with a typical torque (2 Nm) used for screw insertion during anterior cruciate ligament reconstruction, the maximum von Mises and shear stress values were concentrated in the corners or turns of the drive, which could lead to stripping if the values were greater than the yield stress of Mg (193 MPa). With a four-time increase in drive depth to be fully driven and a 30% greater drive width, these maximum stress values were significantly decreased by more than 75%.

Conclusion: It was concluded that improving the design of a Mg-based screw may increase surgical success rates, by decreasing device failure at insertion.

The translational potential of this article: The results of this work have the potential to improve designs of degradable IFSs, allowing for greater torque to be applied and thus greater screw fixation between host bone and the graft. Such a fixation will allow greater integration, better patient healing, and ultimately improved patient outcomes.

Introduction

Following an anterior cruciate ligament (ACL) tear, surgical reconstruction using tendon autografts or allografts as a replacement can stabilize the knee [1]. These grafts are held in place by means of interference screws (IFSs) in the bone tunnel [2]. Two classes of materials, metallic (i.e., titanium) and polymeric (i.e., polylactic acid), are commonly used for the IFSs. Titanium IFSs can provide good initial fixation strength because of its high strength and an elastic modulus on the order of 100 GPa [3,4]. However, there are shortcomings that include magnetic resonance imaging interference, graft laceration resulting from their sharp threads, and the difficulty of removal during revision surgery [5].

* Corresponding author. Department of Chemical, Biological, and Bioengineering, North Carolina A&T State University, Greensboro, NC, USA
E-mail address: mattbm@ncat.edu (M.B.A. McCullough).

https://doi.org/10.1016/j.jot.2019.09.003
Received 29 November 2018; Received in revised form 12 July 2019; Accepted 9 September 2019
Available online 14 October 2019

As a result, polymeric IFSs were developed and gained popularity. Their potential to be bioabsorbable is also an attractive feature. Over time, the screw can be replaced by the bone—soft tissue interface. However, the actual degradation after implantation of these screws was slow, inconsistent, and often incomplete even after two years [6]. In addition, problems with screw breakage during insertion can be frequent [7,8]. Efforts have been made to understand screw-graft performance under postoperative conditions. Chizari et al [9] simulated cyclical loading on the graph-screw construct, using finite element analysis (FEA). Chizari concluded that finite element (FE) models were accurate when compared with experimental values. Additional work, particularly in the area of orthodontics has used FEA to examine the impact of various design factors [10].

In this study, we explored the use of a magnesium (Mg)–based IFS. Mg has several advantages compared with traditional materials including the following: a modulus and tensile strength closer to cortical bone; higher ductility compared with polymers; and high levels of biocompatibility, biodegradability, and osteoconductivity. Mg-based alloys do not interfere with magnetic resonance imaging, allowing better imaging for postoperative assessments [11,12]. Previous work compared the biomechanical characteristics of Mg-based IFS to polymeric screws in cadaveric specimen, and found similar mechanical stability between the two [13]. Such findings suggest that using a degradable Mg-based screw would create similar postoperative outcomes as what is seen in polymeric screws. Initially, a Mg-based IFS of similar design to commercially available titanium screws was tested. ACL reconstruction via graft fixation of a patellar-tendon bone graft was attempted in an *ex vivo* goat model. It was found that stripping and breakage of the screw drive or head occurred during insertion. Previous efforts sought to improve screw drive design in hopes of better performance. Weiler et al compared six bioabsorbable polymer IFSs of similar size with differing drive designs. These authors found that resistance to breakage during insertion was highly dependent on the drive design; specifically, the drive diameter and drive shape [7,8,14–17]. Unfortunately, material properties of the screws were not altered as part of the analysis.

Using the finite element method, the stress distribution within the screw drive was analyzed [18,19]. From these findings, the research question formulated was what are the factors of the screw drive that could be modified to preserve the integrity of the screw? It was hypothesized that an increase in the drive surface area would allow for better distribution of the stresses during screw insertion; and thus, would reduce stripping of the screw drive. To do this, a parametric analysis of drive depth and drive width was performed on a total of six different drive designs. The success criterion was that the level of stress within the screw drive design in response to an applied torque must be 50% lower than the yield strength of the Mg alloy (193 MPa). To the authors' knowledge, this study is the first to examine Mg-based IFS.

Materials and methods

The Mg-based IFS used for this study had a 15 mm length, 5 mm diameter, an inner diameter of 1.73 mm (cannulation), and a 2.51 mm hexagonal drive with a 3.10 mm drive depth (Figure 1). Three-dimensional computer models of the screws were developed using SolidWorks 2010 (SolidWorks Corp., Waltham, MA, USA) computer-aided design software. Finite element analyses were conducted on the models of the screw using ANSYS Workbench 14.0 (ANSYS, Inc., Canonsburg, PA, USA). A convergence study was conducted to determine appropriate number of elements in a model consisting of the titanium screw embedded in the polyurethane foam cylinder. This specific model was used for validation and converged at an element size of 0.80 mm (14,298 tetrahedral elements). Hence, the pullout simulation of screw pullout was run with 14,298 elements.

In lieu of a physical/experimental validation, an algebraic validation of the screw model was conducted using a relationship between pullout strength, thread geometry, and material shear strength [20,21].

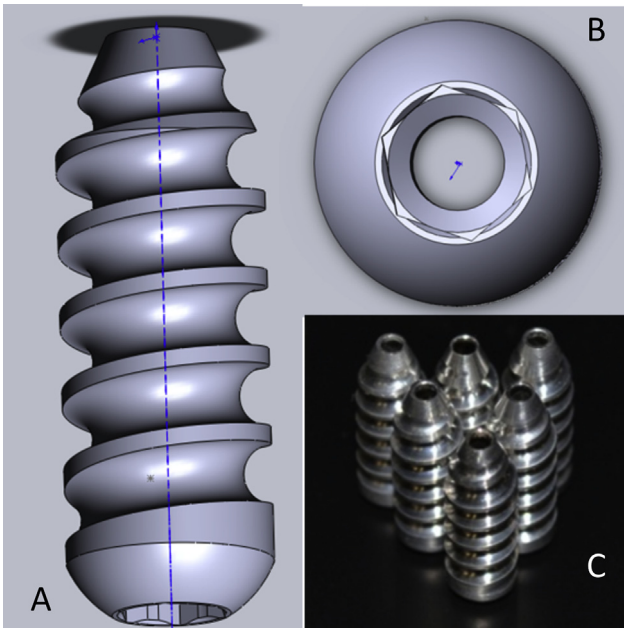

Figure 1. (A) The SolidWorks model of the interference screw with a 15 mm length, 5 mm diameter, an inner diameter of 1.73 mm (cannulation), and a 2.51 mm hexagonal drive with a 3.10 mm drive depth (B) Top view of the SolidWorks model. (C) The actual Mg-based interference screws manufactured with Mg alloy AZ31.

Particularly, Chapman et al determined an algebraic relationship between design parameters and shear failure force in polyurethane foam (Equation 1) [20]. The predicted shear failure force (F_s) is the product of the ultimate shear stress of the material into which the screw is placed (S), length of screw insertion (L), screw circumference (π^*D_{major}, where D_{major} is the major diameter), and the thread shape factor (TSF = 0.5 + 0.57735 d/p, where d is thread depth and p is thread pitch) [20]. Verification of this relationship determined that the aforementioned parameters can be used as predictors of screw pullout force [20].

$$F_s = S^*A_s = (S^*L^*\pi^*D_{major})^*\text{TSF} \quad (1)$$

For validation purposes, S was set to 1.40 MPa, L to 13.36 mm, D_{major} to 5.21 mm, and TSF to 0.75, where d was 0.85 mm and p was 2 mm. Thus, the predicted pullout force as determined from Equation 1 was

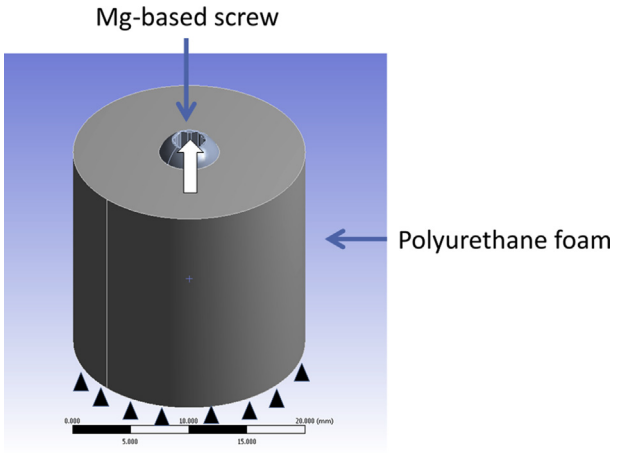

Figure 2. The FE model of the interference screw with Mg alloy material properties embedded in a cylinder having the material properties of 10 pcf polyurethane foam. Black triangles along the bottom of the cylinder represent a fully constrained surface. The white arrow overlaying the screw represents the upward displacement assigned to the screw.

230.12 N. The computational simulation used for validation included a 5 × 15 mm screw embedded in a cylinder with a 20 mm diameter and 20 mm length (Figure 2). The screw was assigned the material properties of titanium alloy as defined by ANSYS 14.0 ($E = 9.60 \times 10^4$ MPa, $\upsilon = 0.36$) [20]. The surrounding cylinder was assigned the material properties of 10 pcf polyurethane foam ($E = 57.0$ MPa, $\upsilon = 0.24$), which is used as a bone substitute for screw pullout testing. Boundary conditions for validation included fixing the bottom surface of the bone block eliminating all movement. The screw was displaced 0.30 mm axially, the displacement at which internal threading of the polyurethane foam cylinder failed. This displacement was determined from initial studies in the authors' laboratory. The coefficient of friction between the screw and the cylinder was 0.42, which is the coefficient of friction between metal and bone [22]. The force resulting from the 0.30 mm displacement of the screw was reported as the pullout force predicted by the computational simulation. The computational pullout force was compared with the predicted pullout force determined by Equation 1 (230.12 N) and the percent difference was calculated.

A comparison study of six different drive designs was performed using the finite element method simulating the loading on the screw drive during insertion. Each model was modified to have each of the following drive designs: hexagonal, quadrangle, torx, trilobe, and turbine (Figure 3). The screws were assigned Mg alloy material properties as defined by ANSYS 14.0 ($E = 4.5 \times 10^4$ MPa, $\upsilon = 0.35$). The screw models were meshed with a 0.1 mm element size (~80,000 tetrahedral elements) as determined from an additional convergence study of the screw model alone. Boundary conditions included fixing the outer threaded surface of the screw, thus restricting translation and rotation in all directions. A 2 Nm torque was applied to the inner surface of the drive of the screw. This torque is within the range of published insertion torques reported for ACL IFSs [8,23–25]. The maximum von Mises stress and maximum shear stress were recorded for each model as well as the stress distribution within the drive design. Also, the surface area of the screw was recorded for each screw model.

Lastly, a parametric study of drive depth and drive width was conducted on all six of the drive designs. A 2^2 factorial design determined the impact of drive depth and drive width on the stress values experienced within the screw drive (Figures 4 and 5). The two levels for drive depth were 3.10 mm, a drive depth of the Mg-based screw that is similar to that of traditional metal screws; and 13.10 mm, a fully driven design as seen with many polymer screws [8]. The drive width was defined as the diameter of the circle in which the drive design is circumscribed. The levels for drive width were 2.30 and 2.90 mm. The drive width of 2.30 mm was half the distance between the cannulation (1.73 mm) and the outer width of the initial Mg-based screw, 2.90 mm. Thus, there were four combinations of drive depth and drive width: (1) 3.1 mm drive depth and 2.3 mm drive width; (2) 3.1 mm drive depth and 2.9 mm drive width; (3) 13.1 mm drive depth and 2.3 mm drive width; and (4) 13.1 mm drive depth and 2.9 mm drive width. As described above, a 2 Nm torque was again applied in the drive of the screw models whose outer threaded surface was fixed. The maximum von Mises stress values were recorded. This was done for a total of 24 combinations of drive design, drive depth, and drive width. The statistical significance of these factors was determined by performing an analysis of variance, where $p < 0.05$ is significant, using SAS version 9.2 (SAS Institute Inc., Cary, NC, USA).

Results

The corresponding stress distributions of the six drive designs (hexagonal, quadrangle, torx, trigonal, trilobe, and turbine) were compared. The maximum von Mises stresses were 196, 209, 212, 197, 245, and 280 MPa, respectively. The maximum shear stresses were 112, 120, 122, 113, 140, and 131 MPa, respectively. Figure 6 shows the von Mises stress concentrations for the screw with a hexagonal drive design with warmer colours (i.e., yellow, orange, red) indicating higher stress values. The maximum stress concentrations were seen in the corners or turns of the drive. The maximum von Mises stress of 196 MPa was greater than the yield strength of the Mg alloy (193 MPa). Thus, failure of the material at the corners of the screw, because of the applied force is highly likely. Von Mises stresses at the corners of the drive exceeded the yield strength of the Mg in all six drive designs with the same drive width (2.9 mm) and drive depth (3.1 mm).

The parametric study was performed to determine the effects of drive depth and drive width on the maximum von Mises stress values. The corresponding surface areas (mm^2) and maximum von Mises stresses (MPa) for each combination with the differing drive designs are listed in Tables 1 and 2, respectively. Combinations 3 and 4 for each of the drive designs yielded maximum von Mises stresses that were below 50% of the yield stress of Mg alloy except combination 3 of the turbine design. Combination 4 of the quadrangle drive design yielded the lowest von Mises stress of 47 MPa closely followed by combination 4 of hexagonal and torx drive designs with maximum von Mises stresses of 48 MPa and 49 MPa, respectively.

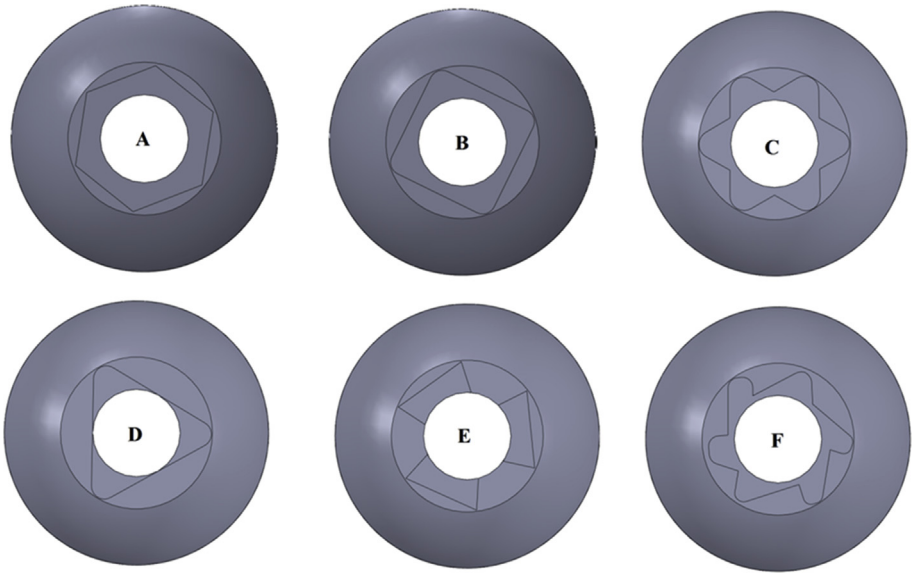

Figure 3. (A) Top view of the hexagonal screw (B) quadrangle screw (C) torx screw (D) trigonal screw and (E) trilobe screw and (F) turbine screw models.

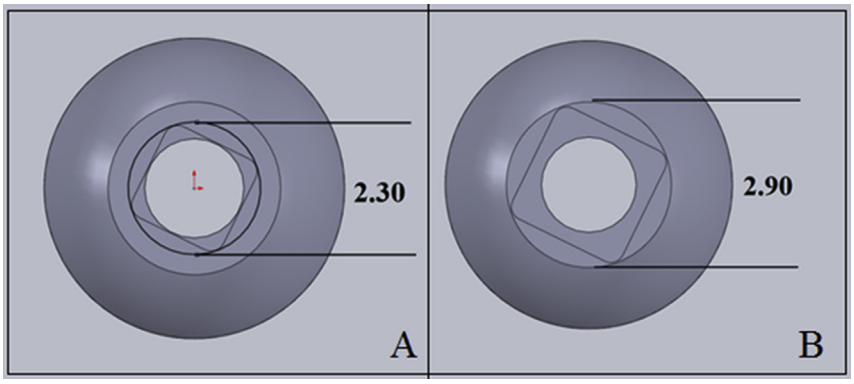

Figure 4. (A) 2.30 mm drive width and (B) 2.90 mm drive width for parametric analysis.

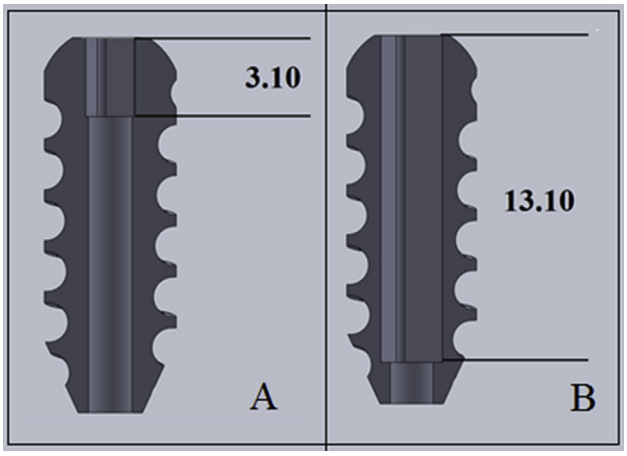

Figure 5. (A) 3.10 mm drive depth and (B) 13.10 mm depth for screw parametric analysis.

For each of the six drive design groups, the maximum von Mises stress decreased approximately 80%. The greatest decrease of 88% was with the trigonal drive design. The parametric study determined that both drive depth and drive width are statistically significant factors having an impact on the maximum stress observed in the model, with p values < 0.0001 and 0.0028, respectively. Overall, there was an inverse relationship between surface area and von Mises stress. Figure 7 shows the relationship of surface area versus maximum von Mises stress for each of the 24 combinations (6 drive designs and 4 combinations of drive depth and drive width) and a greater surface area within the drive of the screw yielded smaller stress values. Using this validated model, a torque applied within the screw drive of the six differing drive designs consistently showed that the concentration of the stress were in the corners and turns of the drive (Figure 6). Because of the applied torque, it was found that the hexagonal drive design had the lowest maximum von Mises stress. It was followed by the trigonal, quadrangle, torx, turbine, and trilobe designs.

Table 1
Surface area (mm^2) of the drives in the different designs of each screw drive.

Screw drive designs	3.1 mm depth 2.3 mm width	3.1 mm depth 2.9 mm width	13.1 mm depth 2.3 mm width	13.1 mm depth 2.9 mm width
Hexagonal	21	27	90	114
Quadrangle	20	26	86	111
Torx	23	31	95	130
Trigonal	9	25	40	104
Trilobe	23	32	96	134
Turbine	31	40	129	171

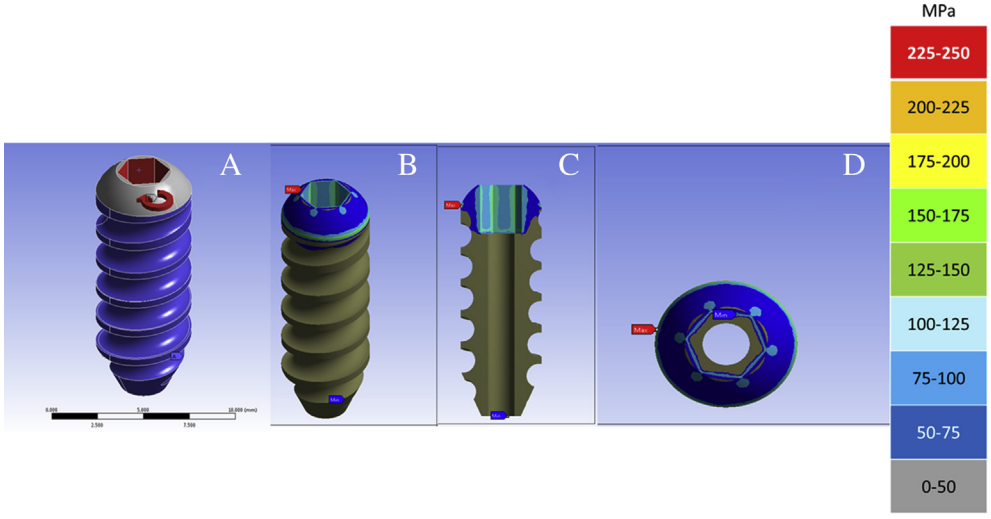

Figure 6. (A) The boundary and loading conditions from the isometric view, (B) Location of the maximal von Mises Stressn (C) A cross section of the location of the maximum von Mises stress (D) Top view of the von Mises plot of the screw model with the hexagonal drive design. The maximum von Mises stress is signified by a red flag, in the corners of the screw drive.

Table 2
Maximum von Mises stress (MPa) of the different designs.

Screw drive designs	3.1 mm depth 2.3 mm width	3.1 mm depth 2.9 mm width	13.1 mm depth 2.3 mm width	13.1 mm depth 2.9 mm width
Hexagonal	224	196	53	48
Quadrangle	298	209	60	47
Torx	246	212	72	49
Trigonal	428	197	95	52
Trilobe	320	245	81	57
Turbine	466	280	141	66

Discussion

The objective of this research was to explore the stress distribution within the screw drive of a Mg-based IFS to better understand the stripping mechanism. An IFS using Mg-based materials has potential advantages over currently available metallic and polymeric screws while aiming to reduce their disadvantages. In this study, Mg-based IFSs were analyzed using a 3-D finite element model. The model was validated in an idealized condition, with a screw embedded in polyurethane foam. The force required to pull the screw out of the foam matched well with results determined from Equation 1. To our knowledge, this is the first study specifically evaluating stresses at the screw drive. This area (i.e., the screw drive) is an important area of study, as physical tests show insertion failure occurring in the head of the screw during implantation.

It was hypothesized that increasing the area of the drive would better distribute stress within the screw. This was confirmed as evidenced by the decreasing values of maximum von Mises stress found in the models. It is worthy to note that in the new screw designs, the maximum stress values were below the level of failure for Mg alloys. There were differences in the stress according to the shape of the drive. This is expected, as different shapes would create different contact areas. Parametric analysis explored the impact of drive depth and drive width on screw performance. Specifically, increasing drive depth four times the current length and increasing drive width by 30%, led to maximum stresses decreasing by more than 75%. These results suggest that drive depth and drive width are factors that would have significant impact on maximum stresses in a screw. Both should be considered when designing a screw with a lower maximum stress and in turn resist drive failure as both yielded statistically significant changes in von Mises stress. In addition, increasing drive depth and width will result in a surface area up to five times greater than the original design. Other means of reducing stripping of the screw include a redesign of the surgical tools. However, it is not clear what the optimal design or material for surgical tools should be because of the variety of Mg alloys used.

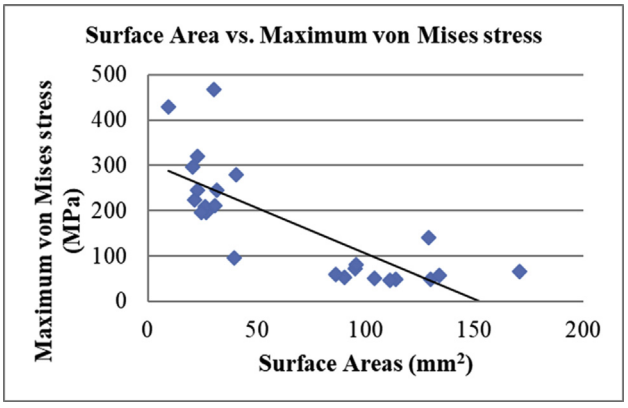

Figure 7. The relationship between surface area and maximum von Mises stress from the parametric analysis including 24 simulations (6 drive designs, 4 combinations of drive depth and drive width each).

This work successfully used FEA to estimate the performance of an IFS during insertion. Results from our study add to current screw design literature centred on what design factors affect the fixation strength of IFSs. The drive was changed to incorporate a fully driven quadrangle design, which has sharper angles to resist the load required for insertion as well as reduce the stress experienced within the drive of the screw. Other investigations of the effect of insertion torque on screw advancement support the methods used here. Multiple studies use a maximum insertion torque ranging from approximately 0.5 to 3.5 Nm [8,23,24,26]. More specifically, Weiler et al investigated how insertion torque affects insertion success, concluding that torque at failure is highly determined by the drive design. The turbine-like drive design had the highest maximum allowable torque followed by the trilobe, quadrangle, trigonal, hexagonal, and torx. For the present study, a similar trend was expected; however, drive designs ranked in the following order from least to greatest maximum von Mises strength: hexagonal, trigonal, quadrangle, torx, turbine, and trilobe. A possible explanation for the difference in results is that Weiler et al used six commercially available polymer screws with different drive designs. These screws were of similar length, but varied in diameter, material properties, thread profile, cannulation, and drive depth. The variability of these factors may have influenced the reported maximum allowable force. For the present study, all the screws had the same material properties, thread design, length, width, cannulation, and drive depth.

There are some limitations to the present study. First, we conducted an algebraic validation of the computation model. For future studies, a physical validation protocol will compare the results obtained from the FEA to the results of an experimental pullout test. Still, the percent difference between the pullout force determined from the computational simulation and the predicted pullout forces was only 5%, which is adequate for validation. Second, the boundary conditions aimed to mimic the experimental protocol do not represent the actually surgical application that includes a soft tissue graft and the surrounding bone. As the external surface of the screw was held fixed, this boundary condition provided more constraints on the screw compared with what is seen clinically. In this analysis, we did not account for the surgical tools nor methods associated with screw insertion. However, the boundary and loading conditions in this study generated the effects of the applied torque in the screw drive. This allowed the model to reasonably predict how the increases in the surface area would reduce the stresses in the screw. Nevertheless, the development of a more complex computational model is a part of our future work. Future studies should analyze the impact of changing material properties on the model. It is expected that materials with higher stiffness will decrease the chances of stripping; however, the combined influence of design and altered material properties will need to be evaluated.

In summary, this study has yielded the first qualitative results of stresses and stress concentration in an Mg-based IFS drive, in response to the torque required during surgery. This is an area that has been limited in its study. Results suggest that when a new material is introduced, new designs must also be considered. As a result, the Mg-based IFS was made fully driven with a quadrangle drive design. A renewed interest in using Mg-based biomaterials for orthopaedic applications is built on the ability of Mg-based alloys to degrade [12]. This degradation eliminates the need for removal surgeries. This work highlights the importance of screw drive design in creating an effective ACL IFS.

Conflict of interest

The authors have no conflicts of interest to disclose in relation to this article.

Funding/support statement

This work was supported by the National Science Foundation, United States of America, Engineering Research Center for Revolutionizing

Metallic Biomaterials (NSF ERC-RMB; grant #0812348) and the National Institute of Health, United States of America training programs: Biomechanics in Regenerative Medicine (BiRM, T32 EB000392) and the Cellular Approaches to Tissue Engineering and Regeneration, United States of America (CATER, T32 EB001026).

References

[1] Smith BA, Livesay GA, Woo S. Biology and biomechanics of the anterior cruciate ligament. Clin Sports Med 1993;12(4):637–70.
[2] Dworsky BD, Jewell BF, Bach Jr BR. Interference screw divergence in endoscopic anterior cruciate ligament reconstruction. Arthrosc J Arthrosc Relat Surg 1996; 12(1):45–9.
[3] Li J, Zhou L, Li Z-c. Microstructures and mechanical properties of a new titanium alloy for surgical implant application. Int J Miner, Metall Mater 2010;17(2):185–91.
[4] Vrouwenvelder WCA, Groot CG, de Groot K. Histological and biochemical evaluation of osteoblasts cultured on bioactive glass, hydroxylapatite, titanium alloy, and stainless steel. J Biomed Mater Res 1993;27(4):465–75.
[5] Bach BR. Observations on interference screw morphologies. Arthrosc J Arthrosc Relat Surg 2000;16(5):E10.
[6] Stähelin AC, Weiler A, Rüfenacht H, Hoffmann R, Geissmann A, Feinstein R. Clinical degradation and biocompatibility of different bioabsorbable interference screws: a report of six cases. Arthrosc J Arthrosc Relat Surg 1997;13(2):238–44.
[7] Barber FA, Elrod BF, McGuire DA, Paulos LE. Preliminary results of an absorbable interference screw. Arthrosc J Arthrosc Relat Surg 1995;11(5):537–48.
[8] Weiler A, Windhagen HJ, Raschke MJ, Laumeyer A, Hoffmann RFG. Biodegradable interference screw fixation exhibits pull-out force and stiffness similar to titanium screws. Am J Sports Med 1998;26(1):119–28.
[9] Chizari M, Snow M, Wang B. Post-operative assessment of an implant fixation in anterior cruciate ligament reconstructive surgery. J Med Syst 2011;35(5):941–7.
[10] Chang JZ-C, Chen Y-J, Tung Y-Y, Chiang Y-Y, Lai EH-H, Chen W-P, et al. Effects of thread depth, taper shape, and taper length on the mechanical properties of mini-implants. Am J Orthod Dentofacial Orthop 2012;141(3):279–88.
[11] Staiger MP, Pietak AM, Huadmai J, Dias G. Magnesium and its alloys as orthopedic biomaterials: a review. Biomaterials 2006;27(9):1728–34.
[12] Tang T-t, Qin L. Translational study of orthopaedic biomaterials and devices. J Orthop Transl 2016;5:69–71.
[13] Song B, Li W, Chen Z, Fu G, Li C, Liu W, et al. Biomechanical comparison of pure magnesium interference screw and polylactic acid polymer interference screw in anterior cruciate ligament reconstruction—a cadaveric experimental study. J Orthop Transl 2017;8:32–9.
[14] Herrera A, Martinez F, Iglesias D, Cegonino J, Ibarz E, Gracia L. Fixation strength of biocomposite wedge interference screw in ACL reconstruction: effect of screw length and tunnel/screw ratio. A controlled laboratory study. BMC Muscoskelet Disord 2010;11(1):139.
[15] Kotani A, Ishii Y. Reconstruction of the anterior cruciate ligament using poly-l-lactide interference screws or titanium screws: a comparative study. The Knee 2001; 8(4):311–5.
[16] Kousa P, Järvinen TLN, Kannus P, Järvinen M. Initial fixation strength of bioabsorbable and titanium interference screws in anterior cruciate ligament reconstruction. Am J Sports Med 2001;29(4):420–5.
[17] Selby JB, Johnson DL, Hester P, Caborn DNM. Effect of screw length on bioabsorbable interference screw fixation in a tibial bone tunnel. Am J Sports Med 2001;29(5):614–9.
[18] Song Y, Debski RE, Musahl V, Thomas M, Woo SL-Y. A three-dimensional finite element model of the human anterior cruciate ligament: a computational analysis with experimental validation. J Biomech 2004;37(3):383–90.
[19] Woo S-Y, Johnson G, Smith B. Mathematical modeling of ligaments and tendons. J Biomech Eng 1993;115(4B):468–73.
[20] Chapman JR, Harrington RM, Lee KM, Anderson PA, Tencer AF, Kowalski D. Factors affecting the pullout strength of cancellous bone screws. J Biomech Eng 1996;118:391–8.
[21] Oberg E, Jones FD, Horton HL. Working strength of bolts. In: Ryffel HH, editor. Machinery's handbook. New York: Industrial Press; 1987. p. 1068–9.
[22] Shirazi-Adl A, Dammak M, Paiement G. Experimental determination of friction characteristics at the trabecular bone/porous-coated metal interface in cementless implants. J Biomed Mater Res 1993;27(2):167–75.
[23] Brand JC, Pienkowski D, Steenlage E, Hamilton D, Johnson DL, Caborn DNM. Interference screw fixation strength of a quadrupled hamstring tendon graft is directly related to bone mineral density and insertion torque. Am J Sports Med 2000;28(5):705–10.
[24] Brown CH, Hecker AT, Hipp JA, Myers ER, Hayes WC. The biomechanics of interference screw fixation of patellar tendon anterior cruciate ligament grafts. Am J Sports Med 1993;21(6):880–6.
[25] Kohn D, Rose C. Primary stability of interference screw fixation. Am J Sports Med 1994;22(3):334–8.
[26] Pena F, Grøntvedt T, Brown GA, Aune AK, Engebretsen L. Comparison of failure strength between metallic and absorbable interference screws. Am J Sports Med 1996;24(3):329–34.